Exotic orbits of two interacting wave sources

S. Protière, S. Bohn, and Y. Couder
Laboratoire Matière et Systèmes Complexes, UMR 7057 CNRS and Université Paris 7-Denis Diderot, Bâtiment Condorcet, Case 7056, 75205 Paris Cedex 13, France

(Received 8 April 2008; revised manuscript received 24 July 2008; published 5 September 2008)

As shown recently, it is possible to create, on a vibrating fluid interface, mobile emitters of Faraday waves [Y. Couder, S. Protière, E. Fort, and A. Boudaoud, Nature **437**, 208 (2005)]. They are formed of droplets bouncing at a subharmonic frequency which couple to the surface waves they emit. The droplet and its wave form a spontaneously propagative structure called a "walker." In the present paper we investigate the large variety of orbital motions exhibited by two interacting walkers having different sizes and velocities. The various resulting orbits which can be circular, oscillating, epicycloidal, or "paired walkers" are defined and characterized. They are shown to result from the wave-mediated interaction of walkers. Their relation to the orbits of other localized dissipative structures is discussed.

DOI: 10.1103/PhysRevE.78.036204 PACS number(s): 05.45.−a, 05.65.+b, 47.55.D−

I. INTRODUCTION

The results we present concern the self-organization of two mobile pointlike emitters having nonlocal interaction through the waves they generate. Before presenting our new results in this domain, we must first recall the origin and main properties of the propagative structure formed by a bouncing droplet and the surface wave it emits.

The existence of such structures relies on the fact that a droplet can be kept bouncing on the surface of a bath of the same fluid if this substrate oscillates vertically. The conditions for which this sustained bouncing is possible were discussed previously [1,2]. During each collision the droplet remains separated from the substrate by an air film. This film does not have time to break before the drop lifts off again. The same process repeats itself so that the drop can be kept bouncing for an unlimited amount of time. At low oscillation amplitude, the droplet bounces at the forcing frequency but for a larger forcing, the vertical motion of the droplet becomes subharmonic. When it has reached this regime, the droplet is observed to start moving horizontally on the fluid interface with a constant velocity [3,4]. This phenomenon occurs when the system is forced with an amplitude below but close to the threshold of the Faraday instability. In the absence of disturbance the interface is flat. The droplet, because of its period-doubled bouncing, becomes a local emitter of Faraday waves which are very weakly damped. The horizontal motion of the droplet is due to a breaking of symmetry. After each jump, the drop falls on the side of the wave it generated at the previous collision. The translation motion of the droplet is thus directly linked to the successive impulsions it receives from bouncing on the wave it has generated. Its velocity v^w is a fraction of the phase velocity v^F of the Faraday waves. We called a "walker" the propagative structure formed by the droplet and its associated wave.

In previous papers the very specific properties of this new type of wave-particle association were explored [5]. In these experiments where the trajectories of the droplets were investigated, it was demonstrated that these trajectories are determined by the propagation of the waves they emit. Being sensitive to the reflection of its own waves on the boundaries, a droplet acquires a kind of nonlocality. Therefore the phenomena specific to wave propagation react on the droplet's motion. It was shown, for instance, that when a walker passes through a slit, the diffraction of its wave results in a probabilistic deflection of the droplet, a phenomenon demonstrating, at a macroscopic scale, a sort of wave-particle duality [5].

When several walkers coexist on the surface of a bath of finite size their motion inevitably brings them close to one another. Even though the droplets do not come directly in contact, they veer off their rectilinear course every time they pass close by. These "collisions" can be of two types. For some values of the collision parameters the walkers repel each other, for others they attract each other. In the former case the two drops have roughly hyperbolic trajectories and the modulus of their velocities is unchanged after the collision. In the latter case the attraction usually leads to a capture where the drops start orbiting around each other. The modulus of the velocity of the droplets is only weakly changed by their orbiting motion. In the limit where the two walkers involved in the collision are identical, these trajectories were studied in detail and the results were reported in a previous paper [4]. This led to understanding and modeling the nature of the interaction. When they pass sufficiently near each other, each of the two droplets bounces on a surface disturbed by the wave emitted by the other. At a given bounce a drop falls on the slope of the wave radially emitted by the other. When it falls on the forward front of this wave the interaction is repulsive, on the backward slope it is attractive. The steady orbiting regime corresponds to a situation where, at all bounces, each drop falls at the same position of the back of the wave emitted by the other. In the present paper we investigate the various types of orbits (see Fig. 1) binding two walkers formed by droplets of different size.

II. EXPERIMENTAL SETUP

The experiments are performed on a liquid bath of thickness $h_0=4$ mm placed in a square container (13×13 cm) submitted to a vertical oscillation with an acceleration $\gamma=\gamma_m\cos(2\pi f_0 t)$. The liquid is a silicon oil with viscosity μ

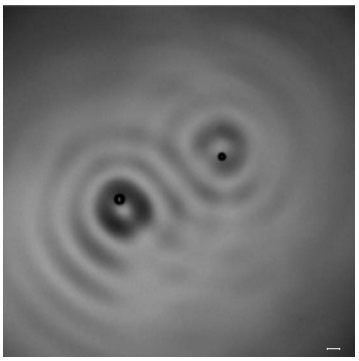

FIG. 1. Photograph of two orbiting walkers of different sizes and velocities bound in an epicycloidal type of orbital motion. The white line represents 1 mm. The waves are localized Faraday waves emitted by the droplets; they have a wavelength $\lambda_F=4.5$ mm. Velocity of the bigger drop: 15 mm/s. Velocity of the smaller drop: 3.2 mm/s.

$=20\times10^{-3}$ Pa s, surface tension $\sigma=0.0209$ N/m, and density $\rho=0.965\,103$ kg m^{-3}. The forcing frequency $f_0=80$ Hz is fixed. With this type of oil, the threshold of the Faraday instability is observed at this frequency for an amplitude of the forcing acceleration: $\gamma_m^F/g=4.2$ (normalized to gravity). The experiments are performed below this threshold for a forcing amplitude $\gamma_m/g=3.8$. The drops are created by dipping a pin in the oscillating bath, then removing it swiftly. The breaking of the liquid bridge between the pin and the bath can generate drops with diameters $0.1<D<1.5$ mm. The drops which are observed to become walkers have diameters $0.5<D<0.9$ mm. We generate two of them on the interface. The lifetime of the drops being long, the same drops can be used for long lasting experiments. We usually wait until the collisions between the drops bind them into an orbital motion. The droplets have two types of motions with different time scales. The bouncing at a frequency $f_F=40$ Hz is observed using a fast camera (with 1000 frames/s). In the horizontal plane, the drops move at velocity v^w, a fraction of the velocity v^F of the Faraday waves. Typically we have $0<v^w\leqslant v^F/10$. In our experimental conditions this means $0<v^w\leqslant 20$ mm/s. Their motion is recorded with a CCD (charged-coupled) camera. We use a semitransparent mirror so as to have a nondistorted image of the surface at normal incidence. A typical image of two orbiting droplets is given in Fig. 1. The films are processed so as to extract from their successive images the trajectories of the drops as well as their velocities.

III. OVERVIEW OF THE VARIOUS SELF-ORGANIZED ORBITS OF TWO DISSIMILAR WALKERS

As previously demonstrated [4] the velocity of a walker is an increasing function of the size of the droplet. At the chosen forcing amplitude two drops of diameter D_1 and D_2 form independent walkers having velocities v_1^w and v_2^w. Just as when they are identical, these walkers can either repel or attract each other. In the latter case they are observed to form a variety of different types of orbits.

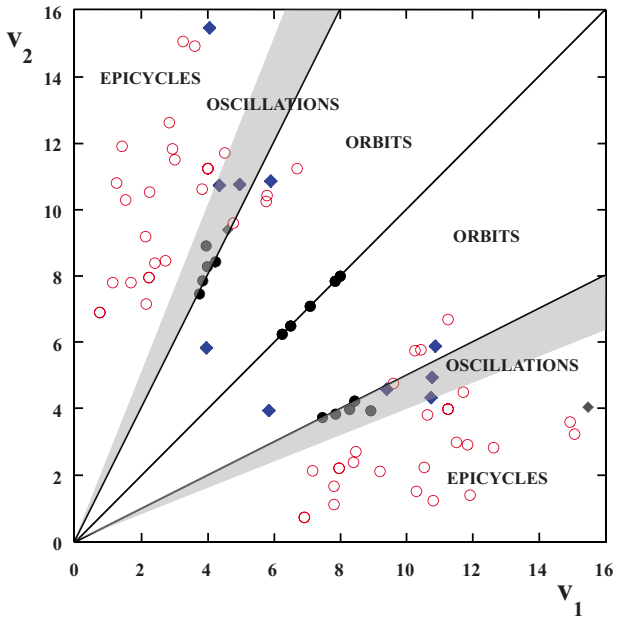

FIG. 2. (Color online) Phase diagram of the different types of orbits observed for two walkers as a function of their two individual velocities v_1 and v_2. Full circles: circular orbits; diamonds: oscillatory orbits; open circles: epicycles. The simple orbital motions are observed in the central region bounded by the lines $v_1=v_2/2$ and $v_2=v_1/2$. The dark gray regions correspond to oscillating orbits. The light gray regions correspond to epicycloidal modes.

Four different types of trajectories are observed. These can be stable circular orbits, oscillating orbits, epicycloidal orbits, or else a type of trajectory, the "paired walkers" mode. We have measured systematically the velocities of various couples of drops and observed their orbits. As can be seen on the phase diagram shown in Fig. 2, the first three types of behaviors are observed in well-defined domains of the parameter space v_1,v_2. The nature of these possible orbits depends on the ratio of their velocities v_1 and v_2. As for the paired walkers mode, it can be observed for practically all velocities v_1 and v_2. We will first describe separately these four types of orbital motion.

A. Circular orbits

Amongst the observed trajectories, the simplest are the stable circular orbits. This type of motion is observed in the central region of the phase diagram of Fig. 2. When the walkers are similar we have $v_1^w=v_2^w$ and the two drops are on the same orbit in a twin-star type of motion. These are the orbits we investigated previously [4] and we shall only recall here the main results. After an attractive collision leading to a capture, two identical walkers form a stable and well-defined orbiting pair, rotating around its center of mass. When bound in orbit, the walkers' velocities are close to what they had been when they were walking freely. In this "ideal" orbiting motion, each droplet bounces on a superposition of its own wave with the wave emitted by the other droplet. The latter provides a force directed along the diameter of the orbit. This force, being transverse, does not con-

tribute to the azimuthal velocity. For this reason the drops, when orbiting, retain approximately the velocity they had as free walkers.

It was also found that the measured diameters of the orbits d_n^{orb} can only take a discrete set of values directly linked to λ_F, the wavelength of the Faraday instability.

$$d_n^{orb} = (n - \epsilon_0^{orb})\lambda_F. \quad (1)$$

Since the drops have a frequency of bouncing half that of the forcing, two drops can bounce either in phase or with opposite phases. In the former case, n can be equal to the successive integers $n=1,2,3\ldots$. In the latter case, the possible values are $1/2,3/2,5/2\ldots$. These values are shifted by an offset ϵ_0^{orb} which is the same for all the possible orbits. The steady orbiting regime corresponds to a situation where, at each bounce, each drop falls at the same position of the back of a wave emitted by the other. The value of the observed offset $\epsilon_0^{orb}=0.2$ shows that the impact is close to the inflexion point of the sinusoid.

The generalization of this type of motion to drops of dissimilar sizes is not straightforward for the following reasons. We now have two drops of velocities v_1^w and v_2^w. Binding them in a circular orbit means that they have to have the same angular velocity ω_0. If the two drops retained their free walkers velocities this would mean that the radii R_1 and R_2 of their orbital motion of the drops would have to be

$$R_1 = v_1^w/\omega_0, \quad (2)$$

$$R_2 = v_2^w/\omega_0. \quad (3)$$

For the interaction to be attractive and of constant modulus, the radii of the orbits should also be such that

$$(R_1 + R_2)_n = (n - \epsilon_0^{orb})\lambda_F. \quad (4)$$

In the case of identical drops all three conditions can be met simultaneously because $v_1^w=v_2^w$ and $R_1=R_2$. However, if the intrinsic velocities of the two walkers are different, there is one equation too many so that all the conditions cannot be met simultaneously. As it turns out the different types of observed orbits correspond to various ways in which one of the conditions given by Eqs. (2)–(4) breaks down.

Stable circular orbits are still observed when the free velocity of one of the walkers is half that of the other, $v_1^w=v_2^w/2$. In this case, the center of rotation is between the two drops (Fig. 3). The fastest walker has the larger orbit. We thus obtain the unusual situation where the center of rotation is closer to the smaller walker.

The condition [Eq. (4)] concerning the sum of the radii still holds. However, the velocities of two orbiting drops are now different from the velocities $v_1^w=v_2^w/2$ they had as free walkers. Figure 4 shows these velocities as a function of the order of the orbit. This is a particularly strong effect (Fig. 4) when the two drops are at the smaller possible distance ($n=0.5$). The small drop's velocity is larger than its velocity as a free walker, whereas the larger drop's velocity is only weakly affected by its binding. For all the other orbits the droplets velocities are always smaller than their velocity when they were free. This effect decreases when the distance between the two drops increases so that the radii of the orbits are then such that $R_1=R_2/2$. The observed shift of the velocities is larger than that which was observed for identical drops [4]. It thus appears that in simple orbits of dissimilar droplets the lock-in on a common angular velocity is obtained mostly by a shift of the velocities of the bound walkers.

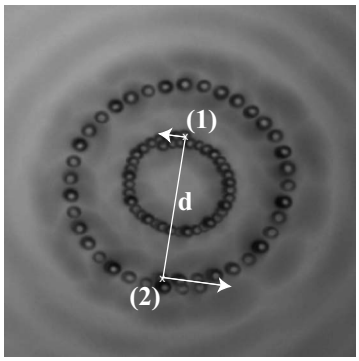

FIG. 3. Superposed images (taken 0.028 s apart) showing the circular orbital trajectories of two dissimilar walkers having a velocity ratio $v_1=v_2/2$ ($v_1=3.7$ mm/s, $v_2=7.5$ mm/s, and $d=8.2$ mm).

B. Oscillatory orbits

When the ratio of the velocities of the two drops is slightly smaller than one half ($0.4<v_1^w/v_2^w<0.5$) the drops still have mean circular trajectories but they also oscillate in the radial direction (see the phase diagram of Fig. 2). The oscillations of the two drops (Fig. 5) have the same frequency but opposite phases. Figure 6 is a plot of the distance d_n^{osc} separating the two drops as a function of time. On the oscillating trajectories shown in Fig. 5, the distance between the two drops can be written as follows:

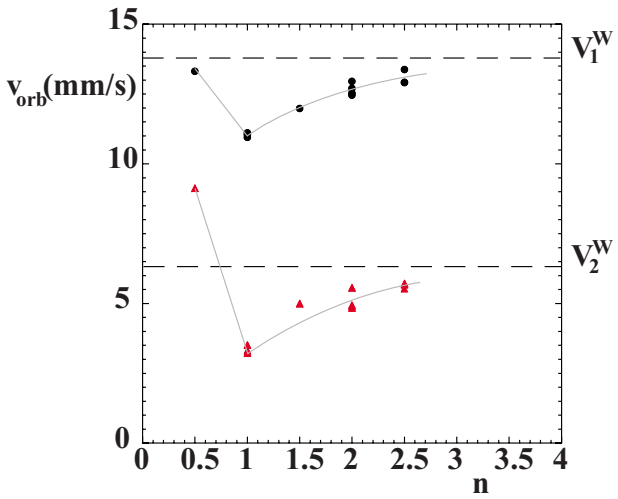

FIG. 4. (Color online) Velocities of two walkers of different sizes as a function of the distance at which they orbit. The dashed lines correspond to their velocities as free walkers: $v_1^w=6.3$ mm/s and $v_2^w=13.7$ mm/s. The gray lines are guides for the eye.

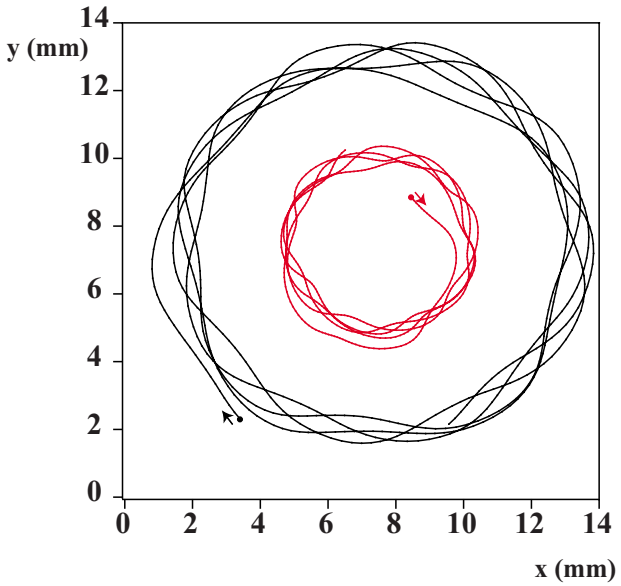

FIG. 5. (Color online) The recorded trajectories of two dissimilar walkers bound in an oscillatory orbit (v_1=4.9 mm/s, v_2 =10.7 mm/s, ω=1.9 rad/s, Ω_{osc}=8.7 rad/s).

$$d_n^{osc} = (n - \epsilon_0 + \epsilon_{osc} \cos \Omega_{osc} t)\lambda_F, \tag{5}$$

with n=2 and ϵ_0=0.2.

This distance varies periodically with a frequency Ω_{osc} which is small compared to the forcing frequency and of the order of 3.5 times the rotation frequency of the walkers. In all the observed oscillating orbits the time average of d_n^{osc} always satisfies the "time averaged" Eq. (5) with ϵ_0 always equal to 0.2. This means that the motion corresponds to an oscillation around one of the discrete stable orbits. The amplitude of this oscillation ϵ_{osc} is always $\epsilon_{osc} < 0.1$ so that d_n^{osc} varies between $(n-0.1)\lambda_F$ and $(n-0.3)\lambda_F$. Each drop still falls on the attractive side of the wave generated by the other.

C. Epicycloidal orbits

When they are very different from each other (v_1^w/v_2^w <0.4), the bound walkers seem, at first glance, to undergo an irregular orbiting motion with strong drifts. The recordings

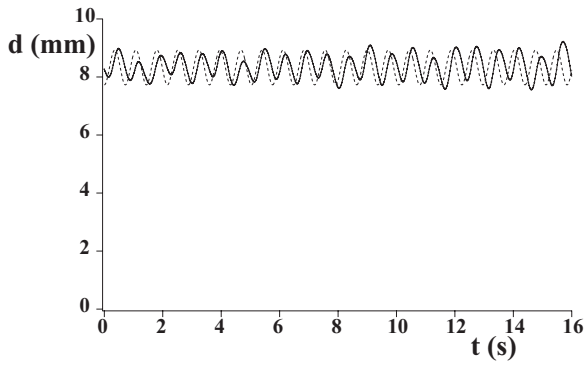

FIG. 6. The oscillation (at frequency Ω_{osc}) of the distance between the two walkers in the oscillating orbit shown in Fig. 5. Solid line: experimental results; dashed line: fit by Eq. (15).

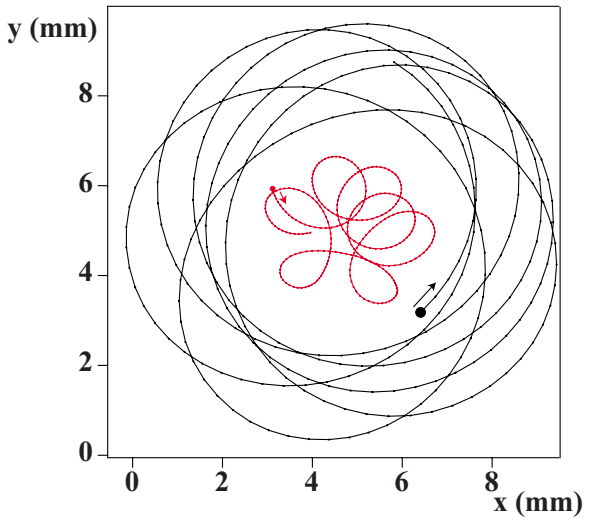

FIG. 7. (Color online) The recorded trajectory of the two walkers having epicycloidal orbits. These are the two walkers shown in Fig. 1, which had free velocities v_1=3.2 mm/s and v_2 =15.1 mm/s, ω=4.3 rad/s, Ω=−0.8 rad/s.

(see Fig. 7), show that the droplets follow well-defined complex trajectories.

These trajectories correspond to coupled hypocycloids or epicycloids. These curves will be defined and characterized below in Sec. IV. Their parameters have been measured and will be given. Despite the fact that most of the observed orbits are really hypocycloids, we will, in the following, use the generic term of epicycloid for this type of orbit. As can be seen on the phase diagram in Fig. 2, they are the only mode observed when the drops have very different intrinsic velocities.

D. Paired walkers

In order to be complete we will finally describe another type of motion observed for all pairs of walkers, provided that their velocities are not too different. In this mode the two droplets walk parallel to each other so that they are strolling together. We called this a "paired walkers" mode. When the two drops are identical they walk together at the same velocity in a straight line, but never for long. They usually oscillate and whenever they come close to a border the pair is dissociated. With two drops of different velocities, each drop retaining its unbound velocity, the pair has a curved trajectory. When the radius of gyration is smaller than the size of our experimental cell this results in a specific type of orbital motion. Both drops are now on the same side of the center of rotation, the fastest drop moving on the larger orbit (Fig. 8).

In this paired walkers mode, as in the other types of orbits, the distance between the two drops is constant and only takes discrete values: d_n^{pair}. We find that it is still proportional to the Faraday wavelength λ_F. In Fig. 9 we find that for a given pair of drops we have $d_n^{pair}=(n-\epsilon_0^{pair})\lambda_F$, with ϵ_0^{pair} =0.32. These results bring about an intriguing question about this type of self-organization. The fact that both drops have a circular motion at a constant velocity means that they are

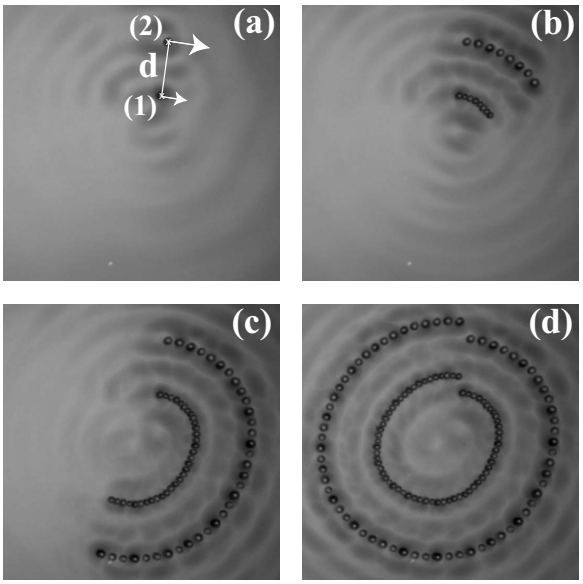

FIG. 8. Superposed images showing the motion of two dissimilar walkers (with $v_1 \approx 4.0$ mm/s, $v_2 \approx 8.2$ mm/s, and $d=5.4$ mm) paired walkers. They have circular trajectories: both droplets being on the same side of the center of rotation.

both submitted to a centripetal force. We thus have here a situation where the fastest drop is attracted by the slower one. But the slower drop has to be repelled by the fastest one. We will give an interpretation of this effect in Sec. V E.

IV. CHARACTERIZATION OF THE EPICYCLOIDAL ORBITS

A. Trajectories of the drops and their fit by epicycles

The experimental trajectories of the type shown in Fig. 7 are well approximated by epicycles, geometrical curves

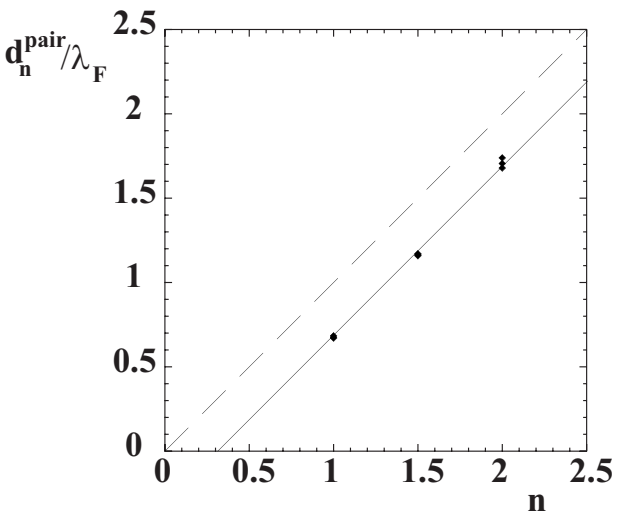

FIG. 9. Distance d_n^{pair} between two drops ($v_1=4.0$ mm/s and $v_2=8.2$ mm/s) orbiting on the same side of the center of rotation as a function of the order n. The straight line corresponds to the best fit with $\epsilon_0^{pair}=0.32$.

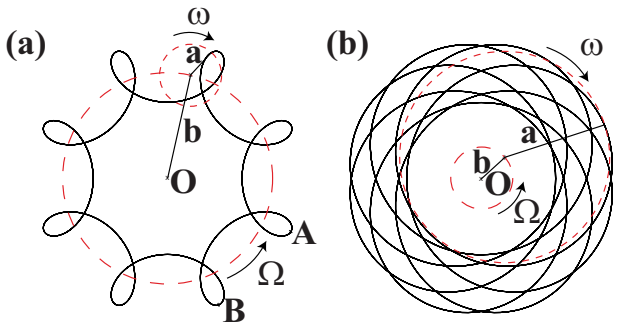

FIG. 10. (Color online) The two types of hypocycles (i.e., where $\omega<0$, $\Omega>0$). In (a) $a<b$ and in (b) $a>b$.

known since antiquity. An epicycle (or a hypocycle) results from the composition of two circular motions. It follows the path of the radius vector of one circle rotating with the angular velocity ω centered on another circle rotating with the angular velocity Ω.

The equation for this curve is given by

$$\vec{r}(t) = a\begin{pmatrix}\cos(\omega t+\phi)\\ \sin(\omega t+\phi)\end{pmatrix} + b\begin{pmatrix}\cos(\Omega t+\Phi)\\ \sin(\Omega t+\Phi)\end{pmatrix}, \qquad (6)$$

where a and b denote the radii of the circles. To simplify the notations we use a description with complex numbers as follows:

$$r(t) = ae^{i(\omega t+\phi)} + be^{i(\Omega t+\Phi)}.$$

We can notice that the trajectory remains the same by a simultaneous exchange of ω for Ω and of a for b. We thus have to make a coherent conventional choice. As we will see below, in all situations the two frequencies ω and Ω are common to the two orbiting droplets. As for the amplitudes a and b, it turns out that one of them is common to the two drops while the other is different. In the following we will systematically choose b to characterize the motion which has the same amplitude for the two drops. For the hypocycloidal and the epicycloidal modes we find that the common oscillation has the smaller angular velocity. For this reason, with this choice of b, we have $|\Omega|<|\omega|$. The first term of Eq. (6) thus corresponds to a rapid rotation and the second to a slower rotation. The directions of rotation of ω and Ω as well as the relative values of a and b define various types of trajectories. Figure 10 shows the hypocycles (where the directions of rotation are opposite to each other). The first graph in (a) corresponds to the case with $a<b$ while the second in (b) shows a hypocycle where $a>b$. In both cases the loops are directed outwards, a characteristic of the hypocycles. If we had chosen the same direction of rotation, we would have observed epicycles and the loops would be turned inward.

Let us now illustrate on one example the determination of the parameters which will give the best fit to a given trajectory. We will first consider the trajectory of the smaller drop of the orbiting pair shown in Fig. 7. This trajectory exhibits seven loops. The drop thus undergoes two rotational motions: one corresponds to each loop, the other to the global motion around the center of the figure. Since the loops are

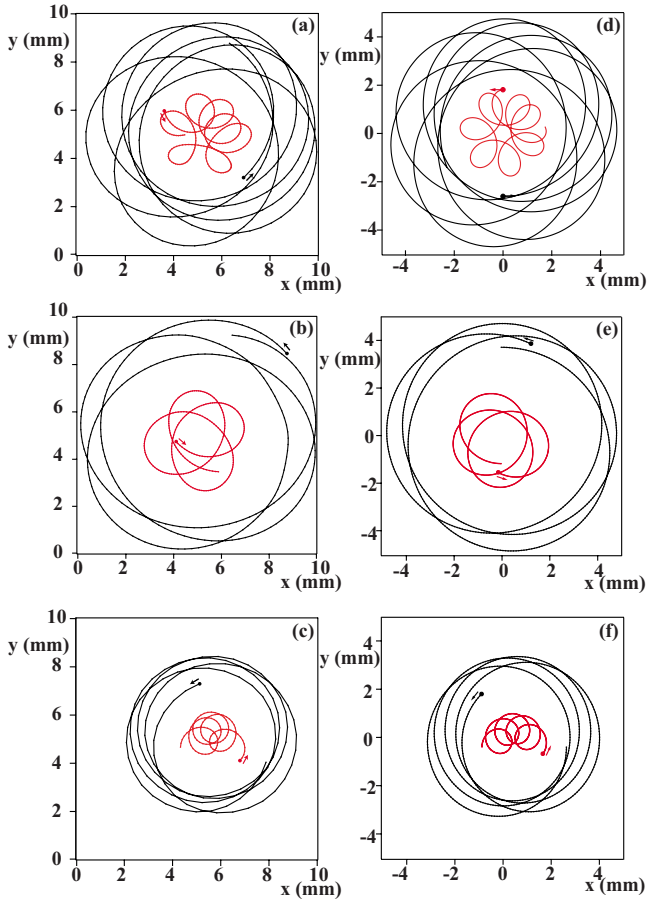

FIG. 11. (Color online) The observed trajectories and their fit by epicycles or hypocycles. Three measured trajectories of pairs of walkers are shown in (a), (b), and (c). In (a) where $v_1=3.2$ mm/s and $v_2=15.1$ mm/s, the two trajectories are hypocycles with $a_1<b<a_2$ ($a_1=0.7$ mm, $a_2=3.6$ mm, and $b=1.1$ mm). In (b) where $v_1=4$ mm/s and $v_2=11.2$ mm/s, the trajectories are also hypocycles with $b<a_1<a_2$ ($a_1=1.5$ mm, $a_2=4.3$ mm, and $b=0.5$ mm). In (c) where $v_1=2.3$ mm/s and $v_2=11.1$ mm/s, the trajectories are epicycles with $a_1<b<a_2$ ($a_1=0.6$ mm, $a_2=2.9$ mm, and $b=0.8$ mm). (d)–(f) show the corresponding trajectories as computed using the equations of epicycles [Eq. (12)].

directed outward, the trajectory is a hypocycle (with $a<b$ the directions of rotation are opposite to each other). We first measure the period T_1 of the global motion around the center: it corresponds to the time needed by the drop to undergo a complete rotation and return to its initial angular position. We thus obtain Ω_1 by $T_1=2\pi/\Omega_1$. We then measure T_1^{loop}, the time the drop needs to go around a single loop of the trajectory. For a hypocycle we then have $T_1^{loop}=2\pi/(\omega_1+\Omega_1)$, from which we deduce ω_1. We obtain the amplitude a_1 and b_1 by measuring the radius of the two envelopes of the global trajectory which are a_1+b_1 and $|a_1-b_1|$, respectively.

The trajectory of the larger drop in Fig. 7 is also a hypocycle but with $a_2>b_2$. We use the same method to measure the parameters ω_2, Ω_2, a_2, and b_2.

B. Correlated motions of the two drops

We now seek a description of the correlation between the motions of the two drops. We measured the trajectories for several pairs undergoing epicycloidal trajectories. Three of them are shown in Fig. 11. In (a) and (b) the trajectories are hypocycles, and in (c) they are epicycles. Even though all these trajectories seem different we can present a simple common description.

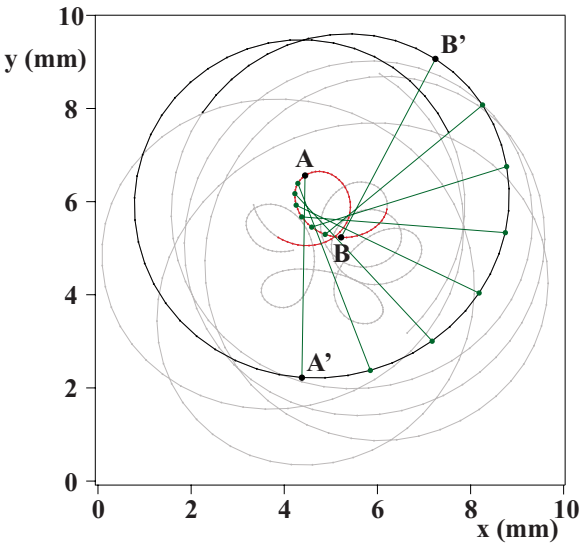

FIG. 12. (Color online) Detail of the motion of the two drops. On a half of one loop of the hypocycle the successive positions of the drops have been marked at regular time intervals. The vector d_{12} has been drawn at these times. When the small drop (1) is in A (at the furthest point of its loop), the large drop is in A', the point of its trajectory closest to the center.

We assume that the trajectories $r_1(t)$ and $r_2(t)$ of drops (1) and (2) can be written in the general form,

$$r_1(t) = a_1 e^{i(\omega_1 t+\phi_1)} + b_1 e^{i(\Omega_1 t+\Phi_1)},$$

$$r_2(t) = a_2 e^{i(\omega_2 t+\phi_2)} + b_2 e^{i(\Omega_2 t+\Phi_2)}. \quad (7)$$

In the experimental reality the two trajectories are coupled and this brings strong constraints on the values of the parameters of Eq. (7).

In Fig. 12 we have singled out one loop of the orbit of Fig. 7 and we have correlated the positions of the two drops at successive times 0.3 s apart. Therefore the distance between the points indicates the drop's velocity. When the small drop is in A, the furthest from the center, its velocity is minimum. At that same time, the other drop is in A', the closest to the center, and its velocity is maximum. As the small drop's velocity decreases, the large drop's velocity increases so that the situation reverses: when the small drop is closest to the center of the figure, the large drop is at the furthest in B'.

Several important differences with the circular orbits can be noted. The line linking the two drops at a given time does not pass through the center of the two epicycles. It is possible to define an instantaneous center of rotation of the two drops. If one traces the two lines between the position of the two drops at times t and $t+\Delta t$, they intersect in a point which

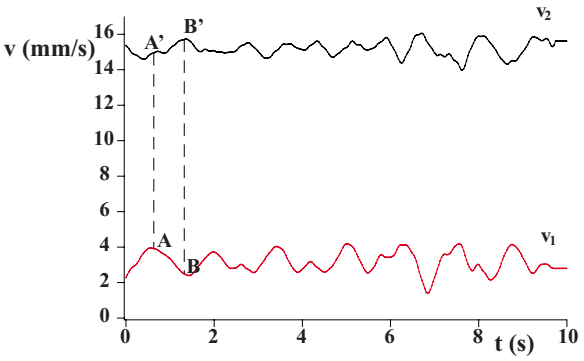

FIG. 13. (Color online) The velocity of two drops of different sizes as they undergo the epicycloidal trajectory obtained in Fig. 11(a). Points A and B and A' and B' correspond to the velocities at the points of the trajectories seen in the previous figure.

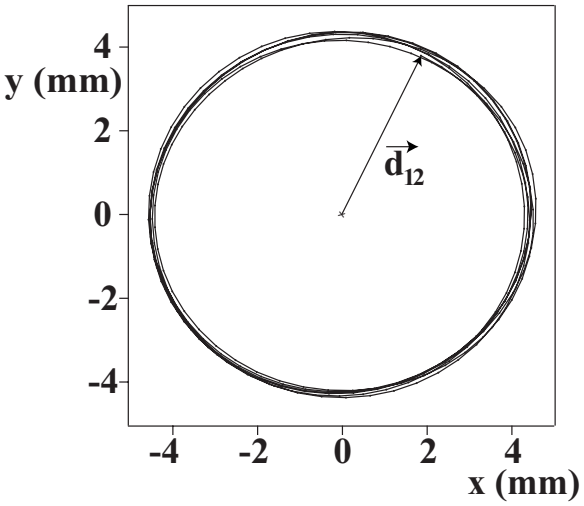

FIG. 14. The time evolution of the vector between the two drops of the previous figure. It has a constant modulus and rotates at a constant angular velocity.

is the instantaneous center of rotation. If we repeat this operation we find that it is not a fixed point. Its locus is also an epicycle.

Another difference with circular orbits concerns the droplets' velocities. Figure 13 shows the two walkers' velocities measured during their trajectories of Fig. 7. When the smallest drop's velocity v_1 is maximum, the largest drop's velocity v_2 is minimum. The points A and B (and A' and B') in this figure correspond to the labeled points of the trajectory in Fig. 13. However, some simple general features of these coupled epicycloidal motions emerge.

Within experimental accuracy, the best fits performed on the two hypocycloidal trajectories of the two drops show that their two angular velocities are the same: $\omega_1=\omega_2=\omega$ and $\Omega_1=\Omega_2=\Omega_{epi}$. Furthermore, the amplitude of the slower component of the motion is also the same: $b_1=b_2=b$.

From the measurements of $\vec{r}_1(t)$ and $\vec{r}_2(t)$, the positions of the two drops as a function of time, we can deduce the vector linking the two drops $\vec{d}_{12}(t)=\vec{r}_2(t)-\vec{r}_1(t)$ (see Fig. 12). Figure 14 shows that for such a complex pair of trajectories as shown in Fig. 11(a), $\vec{d}_{12}(t)$ rotates at constant velocity ω and its modulus; the distance d_n^{epi} between the two walkers remains approximately constant. This result has been observed consistently for all epicycloidal trajectories.

The modulus of the distance between the drops can be deduced from the equations of the epicyles; it can be written as follows:

$$d^2 = a_1^2 + a_2^2 + b_1^2 + b_2^2 - 2[a_1a_2\cos(\phi_1-\phi_2) + b_1b_2\cos(\Phi_1-\Phi_2)] + 2a_1\{b_1\cos[(\omega-\Omega_{epi})t + (\phi_1-\Phi_1)] - b_2\cos[(\omega-\Omega_{epi})t + (\phi_1-\Phi_2)]\} + 2a_2\{b_2\cos[(\omega-\Omega_{epi})t + (\phi_2-\Phi_2)] - b_1\cos[(\Omega_{epi}-\omega)t + (\Phi_1-\phi_2)]\}. \quad (8)$$

For the distance to be constant the time dependent terms have to be zero. This means

$$b_1 = b_2, \quad (9)$$

$$\phi_1 = \phi_2 + \pi, \quad (10)$$

$$\Phi_1 = \Phi_2. \quad (11)$$

The distance between drops is then simply

$$d = a_1 + a_2.$$

Consequently, Eq. (7) of the trajectories of the coupled drops simplify to

$$r_1(t) = a_1e^{i\omega t} + be^{i\Omega_{epi}t},$$

$$r_2(t) = a_2e^{i(\omega t+\pi)} + be^{i\Omega_{epi}t}. \quad (12)$$

As a result, a simple description of the global motion emerges, shown in Fig. 15. These epicycloidal motions can be seen as a simple destabilization of the circular orbits. In first approximation the two drops have their normal circular orbital motion at a frequency ω. Their two different radii of rotation a_1 and a_2 have their origin in their difference in velocity as free walkers. However, the system is not stable and the whole figure drifts on a circular trajectory with a weak angular frequency Ω. The circle on which this advection occurs has a radius b. Figure 15 shows three possible situations. In (a) the advection has an amplitude smaller than that of the orbital motions $b<a_1<a_2$. This corresponds to the situation found experimentally and shown in Fig. 11(b). In Fig. 15(b) we have $a_1<b<a_2$, the situation observed ex-

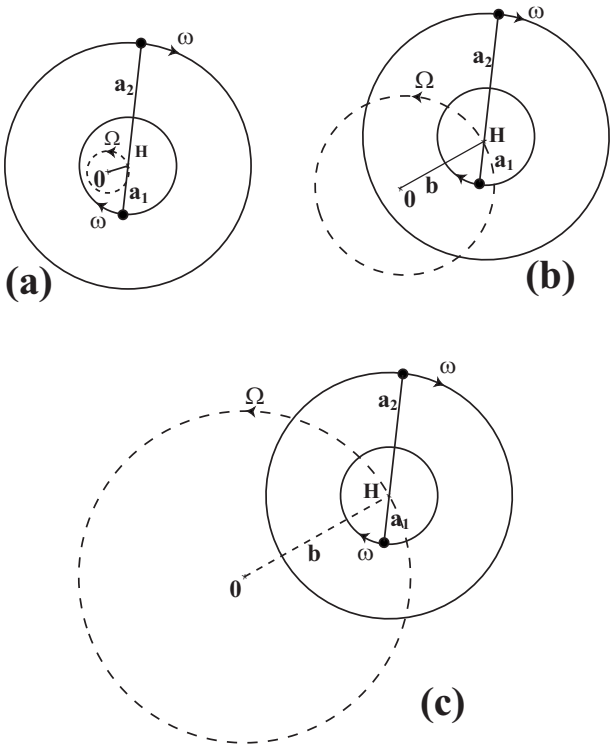

FIG. 15. The various possible types of motion of two drops with hypocycloidal trajectories (i.e., with ω and Ω_{epi} of opposite sign). In (a) the drift is weak, $b<a_1<a_2$. In (b) $a_1<b<a_2$. In (c) the drift is large, $a_1<a_2<b$.

perimentally in Fig. 11(a). In Fig. 15(c) the advection has a large amplitude and $a_1<a_2<b$.

By measuring the remaining parameters we were able to obtain excellent fits to all the epicycloidal orbits that we observed. Some results can be seen in Fig. 11. The three observed trajectories (a), (b), and (c) are well reproduced in (d), (e), and (f), respectively, by setting the measured parameters in Eq. (12).

Using Eq. (12), we can also deduce the velocities of the two bound walkers as follows:

$$|\vec{v_1}(t)|^2 = (\omega a_1)^2 + (\Omega_{epi} b)^2 + 2\omega\Omega_{epi} a_1 b \cos(\omega - \Omega_{epi})t,$$

$$|\vec{v_2}(t)|^2 = (\omega a_2)^2 + (\Omega_{epi} b)^2 - 2\omega\Omega_{epi} a_2 b \cos(\omega - \Omega_{epi})t. \tag{13}$$

These velocities oscillate at the pulsation $\omega - \Omega_{epi}$ around their mean value.

As had been done for circular orbits the same two walkers can be bound in a discrete set of orbits differing by the distance d_n^{epi} separating the droplets. We have measured systematically the possible observed distances by binding repeatedly the same two walkers together. Exactly as for the classical orbiting motion, the distance between the two drops can take discrete values $d_n^{epi} = (n - \epsilon_0^{epi})\lambda_F$ with here $\epsilon_0^{epi} = 0.23$ (see Fig. 16). In spite of the complexity of their trajectories, the two walkers remain bound at a distance linked to λ_F, the Faraday wavelength.

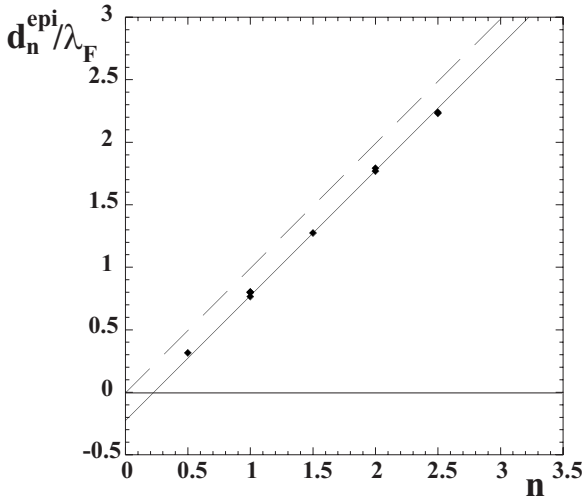

FIG. 16. The normalized distance between the two walkers for various epicycloidal trajectories of different orders n.

We have also observed that for a given pair of drops in an epicycloidal mode, the farther apart the drops are bound, the more solely orbital their trajectories will tend to be. As seen in Fig. 4, when the drops are placed on larger orbits, their velocities increase and tend towards the velocities they each would have as free walkers. This means that the interaction between the drops decreases. We can thus suppose that the stronger the interation between the two drops, the more epicycloidal their trajectories will become. We were not able in this work to find a simple relationship between the two walkers velocities and the resulting parameters b and Ω_{epi} of the trajectories. That would enable us to predict the possible orbits of two given walkers but would require a systematic investigation beyond the scope of the present work.

C. Comparisons of the other orbital modes

All the observed modes of self-organization of two drops comply with a special case of the epicycles equations. The trajectories of two drops on circular orbits correspond to the special case where there is no motion at a second frequency. They are well fitted by Eq. (12) with $b=0$.

$$r_1(t) = a_1 e^{i\omega t},$$

$$r_2(t) = a_2 e^{i(\omega t + \pi)}. \tag{14}$$

In the situation of the oscillating orbits, each of the trajectories can also be fitted by the equation of an epicycloid. The oscillations on the two orbits have the same amplitude. Contrary to the situation previously described, the harmonic motion, which has the same amplitude for the two drops, is now the mode of higher angular velocity. Keeping our convention of choosing b for the common mode, we thus have now $|\Omega_{osc}| > |\omega|$. The two drops oscillate in opposition of the phase. In order to fit the two trajectories, we thus have to add, in Eq. (12), a phase shift π in the term corresponding to the drops' motion at Ω_{osc} as follows:

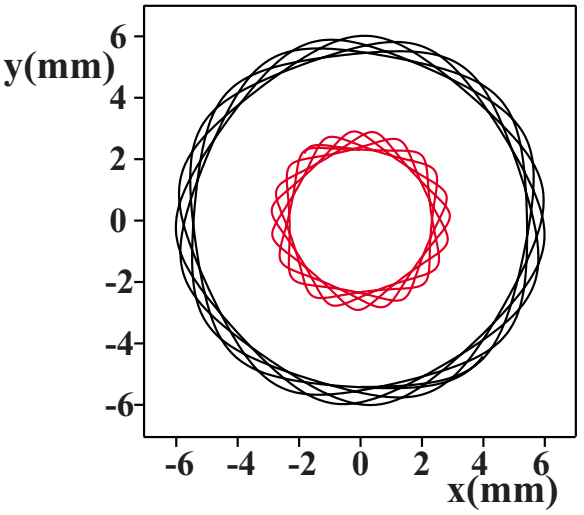

FIG. 17. (Color online) Oscillating orbits of two dissimilar walkers obtained using Eqs. (15) and the parameters a_1=2.6 mm, a_2=5.7 mm, b=0.3 mm, ω=−1.9 rad/s, and Ω_{osc}=6.8 rad/s.

$$r_1(t) = a_1 e^{i\omega t} + b e^{i\Omega_{osc} t},$$

$$r_2(t) = a_2 e^{i(\omega t+\pi)} + b e^{i(\Omega_{osc} t+\pi)}. \quad (15)$$

Figure 17 shows the trajectories drawn using Eqs. (15) and the right parameters so as to match the observed drops' trajectories of Fig. 5. The distance between the two drops is not a constant and its time evolution fits the data (see Fig. 6). The oscillating mode is a kind of high frequency "optical mode" of the two walkers, while the epicycloidal modes would be a low frequency "acoustic mode."

Finally, the paired walkers mode where the two drops are situated on the same side of the center of rotation can also be described using Eqs. (14) but the phase shift π now disappears. We thus have

$$r_1(t) = a_1 e^{i\omega t},$$

$$r_2(t) = a_2 e^{i\omega t}. \quad (16)$$

D. Common features and differences

In circular orbits, or in the paired walkers mode, the center of rotation is fixed and the angular velocity of the motion is constant. The ratio of the velocities and that of the radii of the orbit are the same.

For the two other orbiting modes both the velocities and the radii of rotation vary. For the oscillating trajectories, the center of the trajectories remains fixed so that we choose to consider the mean radii along which the drops orbit. For the epicycloidal trajectories, we can use the instantaneous center of rotation to find the average drop velocities and the average radii of rotations. As shown in Fig. 18, we find that for all types of trajectories the same relation

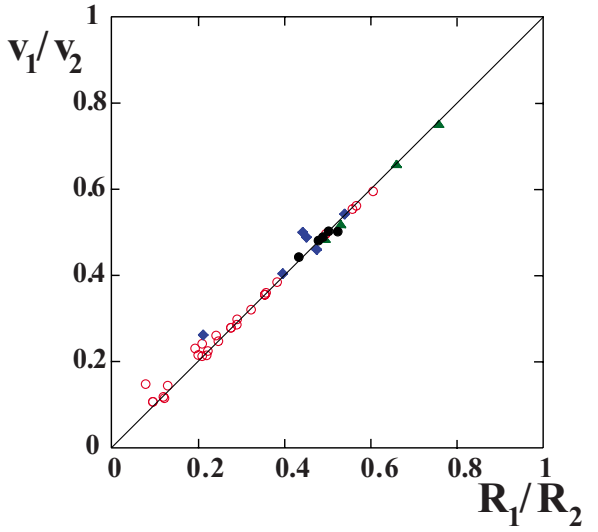

FIG. 18. (Color online) The ratio of the average velocities v_1/v_2 as a function of the ratio of the averaged radii of rotation R_1/R_2. Full circle: circular orbits; diamonds: oscillations; open circles: epicycles; triangle: paired walkers modes.

$$\frac{R_1}{R_2} = \frac{v_1}{v_2} \quad (17)$$

remains valid if average values of the radii and of the velocities are used.

More generally, the drops' interaction via their waves has unusual peculiarities. The barycenter is the point between two objects where they balance each other. It is the center of gravity where two (or more) celestial bodies orbit each other. When a moon orbits a planet, or a planet a star, both bodies are actually orbiting around a point that lies outside the center of the greater body. However, two orbiting drops will place themselves on an orbit in order that their velocities balance each other. Unlike with planets, it is not the drop's mass which determines the radius of its orbit, but its velocity. Here, it is at the velocities' barycenter that the two drops are on a stable orbit. If the velocity varies, then the radius on which each drop orbits varies too.

As for the measured distances between drops, we find that in all modes, except the oscillating orbits, it is constant and can only take a discrete set of values directly linked to λ_F, the wavelength of the Faraday instability, and of the form

$$d_n = (n - \epsilon)\lambda_F. \quad (18)$$

The same holds in oscillating orbits for the average value of d_n.

E. Dynamical origin of the complex orbits

Our measurements have provided an accurate description of the kinematics of the drops motion in the plane of the interface. The underlying dynamics leading to these various organizations results from the droplet-wave interaction. The droplets are the sources of the wave but, in turn, their trajectories result from their bouncing on those waves.

In the following discussion we limit ourselves to two drops bouncing at the Faraday frequency with approximately

the same phase relative to the forcing. The same arguments would hold for drops bouncing with opposite phases.

The simplest case was analyzed previously (see Protière *et al.* [4]) revealing that the interaction can be either repulsive or attractive. In this model, due to Boudaoud, the droplets motion, as well as the forces to which they are submitted, are averaged over a bouncing period T_F. In this limit, two coupled vectorial equations for their positions $\vec{r}_1$ and $\vec{r}_2$ were obtained for the two droplets of masses m_1 and m_2.

$$m_1\ddot{\vec{r}}_1 = F_1^b \sin\left(2\pi\frac{\|\dot{\vec{r}}_1\|}{V_\phi}\right)\frac{\dot{\vec{r}}_1}{\|\dot{\vec{r}}_1\|} + \alpha F_{2\to1}^b \frac{\vec{r}_1-\vec{r}_2}{(\vec{r}_1-\vec{r}_2)^{3/2}}\sin(k_f\|\vec{r}_1-\vec{r}_2\|+\phi_1) - f_1^V\dot{\vec{r}}_1,$$

$$m_2\ddot{\vec{r}}_2 = F_2^b \sin\left(2\pi\frac{\|\dot{\vec{r}}_2\|}{V_\phi}\right)\frac{\dot{\vec{r}}_2}{\|\dot{\vec{r}}_2\|} + \alpha F_{1\to2}^b \frac{\vec{r}_2-\vec{r}_1}{(\vec{r}_2-\vec{r}_1)^{3/2}}\sin(k_f\|\vec{r}_2-\vec{r}_1\|+\phi_2) - f_2^V\dot{\vec{r}}_2. \tag{19}$$

The first term on the right is the effective force exerted on a droplet by bouncing on the inclined surface of its own wave. F_i^b is proportional to the amplitude of the vertical acceleration γ_m and to the slope of the surface waves. The argument of the sine is the phase shift due to the relative displacement of the drop and the wave since the previous collision at velocities $(\vec{r}_i)$ and V_F^ϕ, respectively. The third term stands for the viscous damping due to the shearing of the air layer between the drop and the bath during the contact.

The second term of each equation accounts for the force exerted on one droplet by its bouncing on the wave emitted by the other. The parameter α accounts for the damping of the wave. In the numerical integration of these ODEs the spatially oscillating character of the interaction is retrieved. In the limit where the two droplets are identical, circular orbits are analytical solutions of this set of equations. In these solutions, the velocity of each drop is constant and equal to the velocity it would have as a walker. In the radial direction, equating the force due to the interaction term to the centrifugal effect yields a condition on the possible orbital diameters d_n^{orb} so that the observed discrete set of solutions is retrieved.

With two unequal drops the differences in the observed orbits can be ascribed to several origins. The waves emitted by the two droplets differ in amplitude, in phase, and the collisions with the interface are not simultaneous.

As seen in Fig. 1 the bouncing of the larger drop is a stronger disturbance of the interface so that it is the source of a wave of larger amplitude. Since they modeled successfully the circular orbits, we tried to obtain exotic orbits in the framework of Eqs. (19). In order to take into account the difference in amplitudes of the waves generated by the droplets we set in Eqs. (19): $F_2^b > F_1^b$, $f_2^V > f_1^V$, and $F_{2\to2}^b > F_{1\to2}^b$. Furthermore we tried to account for different times of landing by introducing two different phases ϕ_1 and ϕ_2 in the interaction terms of the equations. These simulations did not permit one to retrieve the exotic orbits described here. The simulations we did convinced us that the model given by Eqs. (19) is oversimplified for this purpose because it does not take into account the temporal variation of the wave amplitudes during the periodic forcing. An improved version should include a more realistic description of the space and time evolution of the waves as well as a better description of the collision itself. This is beyond the scope of the present paper. We will limit ourselves to a qualitative discussion of the observed phenomenology.

The main effect responsible for the qualitative difference of the orbits can be observed in Fig. 19. Two drops of different size do not impact the surface of the liquid exactly at the same time. It is observed that, in the walker regime, a small drop jumps higher than a big one and stays longer in the air. The origin of this difference lays in the elastic behavior of smaller drops which manifests itself also on the threshold of their bouncing [4]. As a result, the collision of the smaller drop with the interface is retarded as compared to the larger one. The smaller drop thus falls on a wave which has propagated a little further away from its source.

A consequence of this type of asymmetry is particularly clear in the paired walkers mode. The circular motion shown in Fig. 8 can only be understood if the drops are submitted to a centripetal force. Since both drops are on the same side of the center of rotation this means that the big drop is attracted to the small one, while the small drop is repelled by the big one. We can understand this phenomenon as an effect of the nonsynchronous collisions of the drops with the interface. The two sketches of Fig. 20 represent the situation at the two instants when the drops collide with the surface. The bigger drop touches the surface on the attractive side of the wave generated by the small drop. When the small drop impacts the surface, the wave formed by the large drop has had more time to propagate so that the impact takes place on the "repulsive" side of the wave.

For two drops in an epicycloidal or orbital mode, the slopes on which each drop falls are both directed toward the other drop. The attractive slope generates the centripetal force necessary to the orbiting motion. In the circular orbits the drops always impact the same slope. However, the epicycloidlike mode must be due to the slow temporal evolution of both slopes. This makes both drops' velocities vary continuously. We can thus associate this slow variation of the slopes to the phase shift between the two drops.

V. DISCUSSION AND CONCLUSION

In the present work, using bouncing drops as local exciters of a system tuned slightly below the threshold of the Faraday instability, we obtain pointlike mobile sources of Faraday waves. We thus excite a localized packet of damped linear waves in the vicinity of a supercritical bifurcation. The resulting objects have nonlocal interactions through the decreasing exponential tail of waves surrounding them. These

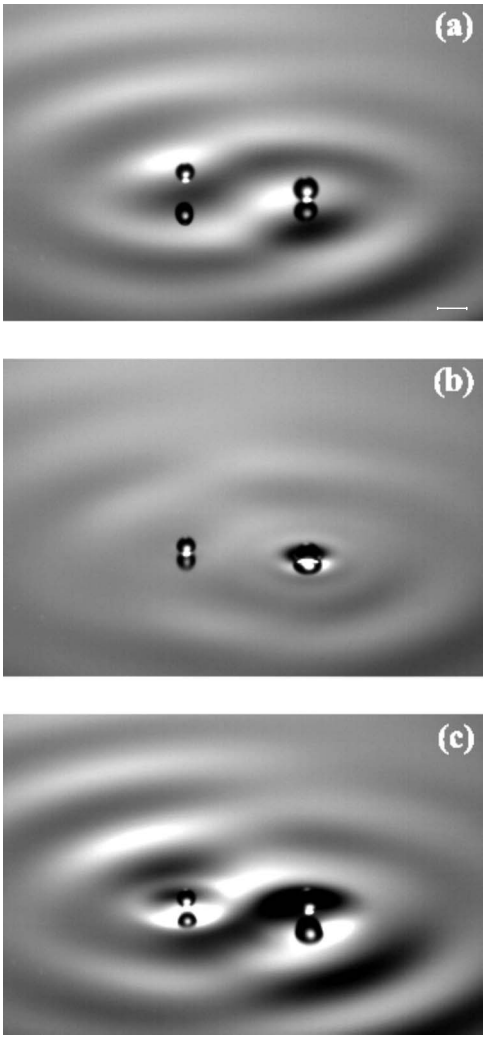

FIG. 19. Three photographs extracted from a fast camera recording of the bouncing of two walkers of different size bound in a hypocycloidal orbit. The white line represents 1 mm. The first photograph is taken at the time t of the first contact of the larger drop with the interface. The second one, 10 ms later, corresponds to the time $t+\delta t$ of the first contact of the smaller drop. On the third photograph (5 mm later) the small drop has already taken off while the large one has not.

modes of self-organization are related to those of the other types of localized structures observed in nonlinear physics.

Isolated localized states are usually associated with subcritical bifurcations. They are observed after a decrease of the control parameter when its value remains constant in the hysteretic region of the bifurcation. In this case, while most of the medium relaxes to the basic state, small domains (usually called localized states) remain in the bifurcated state. When the transition is a subcritical Hopf bifurcation the small domains are oscillatory structures. They are surrounded, in the quiescent region, by a tail of exponentially decaying waves.

These phenomena were first investigated in model equations (e.g., by Aranson *et al.* [6] and Moskalenko *et al.* [7]). They were also investigated theoretically and experimentally in the context of nonlinear optics [8–10] or in reaction-diffusion systems [11,12].

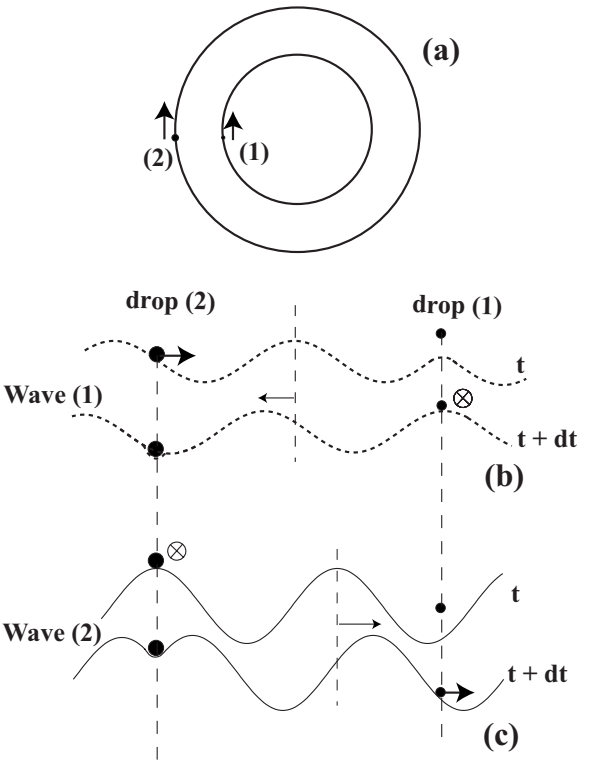

FIG. 20. (a) Sketch of a circular paired walkers mode. (b) Radial profile of the wave created by drop (1) at the times t and $t+\delta t$ when the drops (2) and (1) collide with the interface respectively. By their interaction with this wave, drop (1) is pushed azimuthally (to the back of the figure) and drop (2) is attracted towards the center of the orbit. (c) Radial profile of the wave created by drop (1) at the same times t and $t+\delta t$. By their interaction with this wave, drop (2) is pushed azimuthally and drop (1) is repelled towards the center of the orbit.

Localized structures were previously observed in the Faraday instability in cases where the transition is subcritical as in, for example, vibrated sand by Umbanhowar *et al.* [13] or by Lioubashevski *et al.* in thin layers of suspensions or very viscous fluids [14]. In sand, where they were called oscillons [13], they have short range interaction leading to their aggregation. In fluids Lioubashevski *et al.* [14,15] observed the formation of highly dissipative localized structures with a core region having a complex structure. These structures can become spontaneously propagative. The presence of small amplitude waves around these localized states is sufficient to create an interaction between them [16,17]. They have particlelike interactions which lead to their static aggregation or to orbital motions. The nonlocal interaction mediated by waves is the common factor of our experiment and of these other types of localized objects. This is the origin of the self-organization of circular orbits in both types of systems. The more complex orbits investigated here were not observed in other systems.

We can note, however, that epicycloidal orbits have been observed in a different type of wave-dominated system. When the oscillating Belousov-Zhabotinsky chemical reaction occurs in a spatially extended system it leads to spontaneous formation of spiral waves. While the normal spiral has

a constant rotation it was shown that in some regimes the tip of the spiral starts "meandering." Li *et al.* [18] have studied the motion of the tip. They show that the spiral's tip does not have an erratic motion but rather moves in epicycloidal orbits and that there exists a domain where a bifurcation from simple rotating spirals to meandering spirals occur. Schrader *et al.* [19] have also observed these meandering spiral waves in a periodically excited medium and found these same epicycloidal trajectories.

Our investigation was limited to the orbits of two walkers. When more than two walkers coexist on the surface of the bath an even larger diversity of situations is observed. When the walking threshold is passed while several drops are bouncing independently, each of them becomes a walker and we thus form a "gas" of independent walkers. Some of their collisions lead to capture so that the transient formation of orbiting pairs is observed. These pairs are usually destroyed by the collision of solitary walkers. The formation of orbits with more than two walkers remains exceptional in that case.

However, it is possible to start with different initial conditions. Below the walking threshold, bouncing drops tend to drift towards each other and to aggregate in clusters with a crystal-like structure [4]. The simultaneous transition to walking can then lead to the formation of orbiting structures involving a larger number of droplets. Though beyond the scope of the present paper, we can note that they present the same building rules found in the case of two particles.

ACKNOWLEDGMENTS

We are grateful to Laurent Quartier, Mathieu Receveur, and Alain Roger for their help in setting up this experiment and to Arezki Boudaoud, Sylvain Courrech du Pont, Emmanuel Fort, and Maurice Rossi for many enlightening discussions. This work was supported by the ANR Blanche 02 97/01.

[1] Y. Couder, E. Fort, C.-H. Gautier, and A. Boudaoud, Phys. Rev. Lett. **94**, 177801 (2005).
[2] D. Terwagne, N. Vandewalle, and S. Dorbolo, Phys. Rev. E **76**, 056311 (2007).
[3] Y. Couder, S. Protière, E. Fort, and A. Boudaoud, Nature (London) **437**, 208 (2005).
[4] S. Protière, A. Boudaoud, and Y. Couder, J. Fluid Mech. **554**, 85 (2006).
[5] Y. Couder and E. Fort, Phys. Rev. Lett. **97**, 154101 (2006).
[6] I. S. Aranson, K. A. Gorshkov, A. S. Lomov, and M. I. Rabinovich, Physica D **43**, 435 (1990).
[7] A. S. Moskalenko, A. W. Liehr, and H.-G. Purwins, Europhys. Lett. **63**, 361 (2003).
[8] B. Schapers, M. Feldmann, T. Ackemann, and W. Lange, Phys. Rev. Lett. **85**, 748 (2000).
[9] A. S. Desyatnikov and Y. S. Kivshar, Phys. Rev. Lett. **88**, 053901 (2002).
[10] A. G. Vladimirov, J. M. McSloy, D. V. Skryabin, and W. J. Firth, Phys. Rev. E **65**, 046606 (2002).
[11] C. P. Schenk, P. Schütz, M. Bode, and H. G. Purwins, Phys. Rev. E **57**, 6480 (1998).
[12] A. W. Liehr, A. S. Moskalenko, Y. A. Astrov, M. Bode, and H. G. Purwins, Eur. Phys. J. B **37**, 199 (2004).
[13] P. B. Umbanhowar, F. Melo, and H. L. Swinney, Nature (London) **382**, 793 (1996).
[14] O. Lioubashevski, H. Arbell, and J. Fineberg, Phys. Rev. Lett. **76**, 3959 (1996).
[15] O. Lioubashevski, Y. Hamiel, A. Agnon, Z. Reches, and J. Fineberg, Phys. Rev. Lett. **83**, 3190 (1999).
[16] P. B. Umbanhowar, F. Melo, and H. L. Swinney, Physica A **249**, 1 (1998).
[17] H. Arbell and J. Fineberg, Phys. Rev. Lett. **85**, 756 (2000).
[18] G. Li, Q. Ouyang, V. Petrov, and H. L. Swinney, Phys. Rev. Lett. **77**, 2105 (1996).
[19] A. Schrader, M. Braune, and H. Engel, Phys. Rev. E **52**, 98 (1995).